Available online at www.sciencedirect.com
SCIENCE DIRECT®
International Journal of Refractory Metals & Hard Materials 23 (2005) 91–97
International Journal of REFRACTORY METALS & HARD MATERIALS
www.elsevier.com/locate/ijrmhm

Infrared brazing of Mo using the 70Au–22Ni–8Pd alloy

D.W. Liaw [a], R.K. Shiue [b,*]

[a] Department of Materials Science and Engineering, National Dong Hwa University, Hualien 974, Taiwan, ROC
[b] Department of Materials Science and Engineering, National Taiwan University, Taipei 106, Taiwan, ROC

Received 17 August 2004; accepted 28 October 2004

Abstract

Infrared brazing of Mo using the 70Au–22Ni–8Pd braze alloy is performed in the experiment. Both Au-rich and Ni-rich phases are observed in the infrared brazed joint at 1050 °C. The Au in the molten braze is not reacted with the Mo substrate, but the Ni in the braze preferentially reacts with the Mo. With increasing the brazing temperature and/or time, the interfacial reaction between the molten braze and Mo substrate is greatly enhanced, and the angular MoNi intermetallic compound is formed in the brazed joint, especially for the furnace brazed specimen due to its slow thermal history. The formation of interfacial MoNi intermetallic compound in the brazed joint is detrimental to its bonding strength. Cleavage dominated fracture is widely observed from the fractograph of furnace brazed specimen. Additionally, the application of rapid infrared brazing is a very effective process to inhibit excessive growth of the interfacial MoNi phase in the joint.

Keywords: Infrared brazing; Interface; Molybdenum; Metals and alloys; Microstructure

1. Introduction

Molybdenum is a type of refractory metals due to its melting point exceeding 2450 °C [1,2]. The use of the refractory metals is widely applied in the aircraft, defense, space and nuclear industries [2]. Developing appropriate joining process for metals is indispensable for structural applications. Brazing is accepted as one of methods in bonding assemblies made from refractory metals due to its limited effect on base-metal properties [3]. Refractory metals must be brazed at temperatures below those at which recrystallization occur for maximum strength. Copper and silver-base braze alloys have been previously applied in brazing refractory metals for low-temperature service [3–6]. Additionally, it has also been reported that the single crystal molybdenum is successfully brazed by using Pd, Pd–20Ag and Mo–40Ru for high temperature applications [7–9]. In contrast, the gold-based braze alloy is suitable for medium service temperatures. It is selected as the filler metal in brazing pure molybdenum.

Infrared brazing is featured with fast heating rate up to 3000 °C/min, which is much higher than that of traditional furnace brazing [10–12]. It is an innovative brazing process due to its very rapid thermal history. This research is concentrated on vacuum brazing of molybdenum using the 70Au–22Ni–8Pd braze alloy. Both traditional furnace brazing and infrared brazing are performed in the study. The wettability test, microstructural evolution and shear strength of the brazed joint with various brazing conditions have been widely evaluated in the experiment.

2. Experimental procedures

The base metal used in the test was the pure molybdenum rod. It was machined into the brazing specimen

* Corresponding author Tel.: +886 2 27023069; fax: +886 2 23634562.
E-mail address: rkshiue@ntu.edu.tw (R.K. Shiue).

0263-4368/$ - see front matter © 2004 Elsevier Ltd. All rights reserved.
doi:10.1016/j.ijrmhm.2004.10.003

with dimension of 10 mm × 10 mm × 3 mm. The substrate was polished with SiC papers up to 1200 grit, and subsequently cleaned using an ultrasonic bath with acetone as the fluid prior to the brazing experiment. Palniro-7 foil with 50 μm thick and 25 mm wide was purchased from Wesgo Metals Inc. Its nominal composition in weight percent is 22% Ni, 8% Pd and Au balance. Additionally, the chemical composition of the Palniro-7 braze alloy is in accordance with the BAu-6 braze alloy specified by the American Welding Society (AWS) [3]. Its solidus and liquidus temperatures are 1010 and 1045 °C, respectively. The recommended brazing range of 70Au–22Ni–8Pd alloy is between 1045 and 1120 °C.

Dynamic wetting angle tests were employed using a conventional vacuum furnace with various temperatures for 0–2400 s, respectively [4–6]. The braze alloy with near spherical shape used in the wetting angle test was prepared from 70Au–22Ni–8Pd foil by vacuum arc remelting (VAR) with the operation voltage of 60 V and 130–150 A. The weight of each spherical ball was kept at 0.12 g [4–6]. The spherical ball was placed on the molybdenum substrate, and images of the molten braze on the substrate were recorded simultaneously using an Olympus C-5050 digital camera during the wetting angle measurement.

Both furnace and infrared brazing were performed in the experiment with a vacuum of 5×10^{-3} Pa at various brazing conditions. The heating rate of conventional vacuum furnace was 0.5 °C/s, and the heating rate of infrared furnace was kept at 10 °C/s throughout the experiment. Additionally, all brazed specimens were preheated at 600 °C for 600 s before the brazing temperature was attained. Table 1 summarizes all brazing conditions applied in the test.

The cross-section of the brazed specimen was examined using a Hitachi 3500H scanning electron microscope (SEM) with the accelerating voltage of 20 kV. Chemical analyses were performed using energy-dispersive X-ray spectrometer (EDS) with an operation voltage of 20 kV and minimum spot size of 1 μm. Shear tests were employed using a Shimadzu AG-10 universal testing machine with a constant crosshead speed of 0.5 mm/min compressed the brazed specimens [10–12]. Failure analyses of the brazed specimen after shear tests were inspected using an SEM.

Table 1
Summary of brazing variables used in the experiment

Composition of braze alloys (wt%)	70Ag–22Ni–8Pd
Furnace brazing temperature (°C)	1050
Furnace brazing time (s)	1200
Infrared brazing temperature (°C)	1050, 1100
Infrared brazing time (s)	90, 180, 300

3. Results and discussion

Fig. 1 displays the dynamic wetting angle measurements of 70Au–22Ni–8Pd alloy on the molybdenum substrate at 1070 °C and 1100 °C for 0–2400 seconds, respectively. According to the figure, the molten braze alloy can completely wet the Mo substrate at 1070 °C in 300 seconds. Additionally, increasing the test temperature has little effect in further improving wettability of the molten braze on the substrate.

Fig. 2 displays the SEM secondary electron image (SEI), backscattered electron image (BEI) and chemical analysis results of the furnace brazed Mo/70Au–22Ni–8Pd/Mo specimen at 1050 °C for 1200 s. According to the EDS analysis results, the furnace brazed joint primarily consists of Au-rich and Ni-rich matrix and angular MoNi intermetallic compound. Additionally, the location of huge angular MoNi intermetallics (marked by point C in Fig. 2) is close to the interface between the braze alloy and Mo substrate. The Au-rich phase (marked by B) is alloyed with Ni and Pd as marked by B in Fig. 2, and there is no Mo content detected in the EDS chemical analysis. In contrast, the Ni-rich phase (marked by A) is alloyed with Au, Pd and minor Mo. The Au–Ni–Pd ternary alloy phase diagram is cited here in order to unveil the microstructural evolution of the brazed joint.

Fig. 3(a) shows the liquidus projection of Au–Ni–Pd ternary alloy phase diagrams, and Fig. 3(b) is the isothermal section of Au–Ni–Pd at 300 °C [13]. Both Fig. 3(a) and (b) are in atomic percent. The chemical composition of the braze alloy in atomic percent is 44.1% Au, 46.5% Ni and 9.4% Pd as marked by point B in Fig. 3(b). According to the isothermal section of Au–Ni–Pd at 300 °C, the braze alloy tends to separate into two phases, the Au-rich and Ni-rich phases [13]. Fig. 4 shows the 10 wt% Pd vertical section of Au–Ni–Pd pseudo-binary phase diagram [13]. The atom percent Pd varied

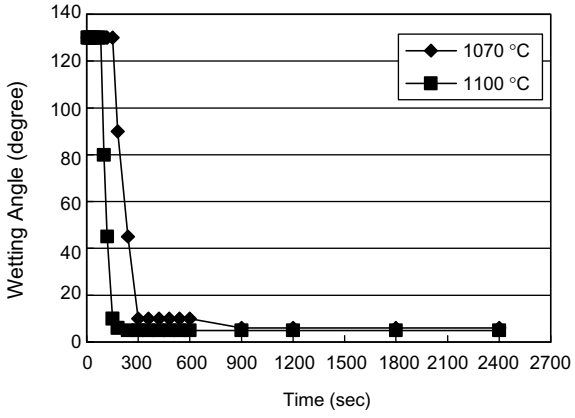

Fig. 1. The dynamic wetting angle measurements of 70Au–22Ni–8Pd alloy on molybdenum substrate at 1070 °C and 1100 °C for 0–2400 s.

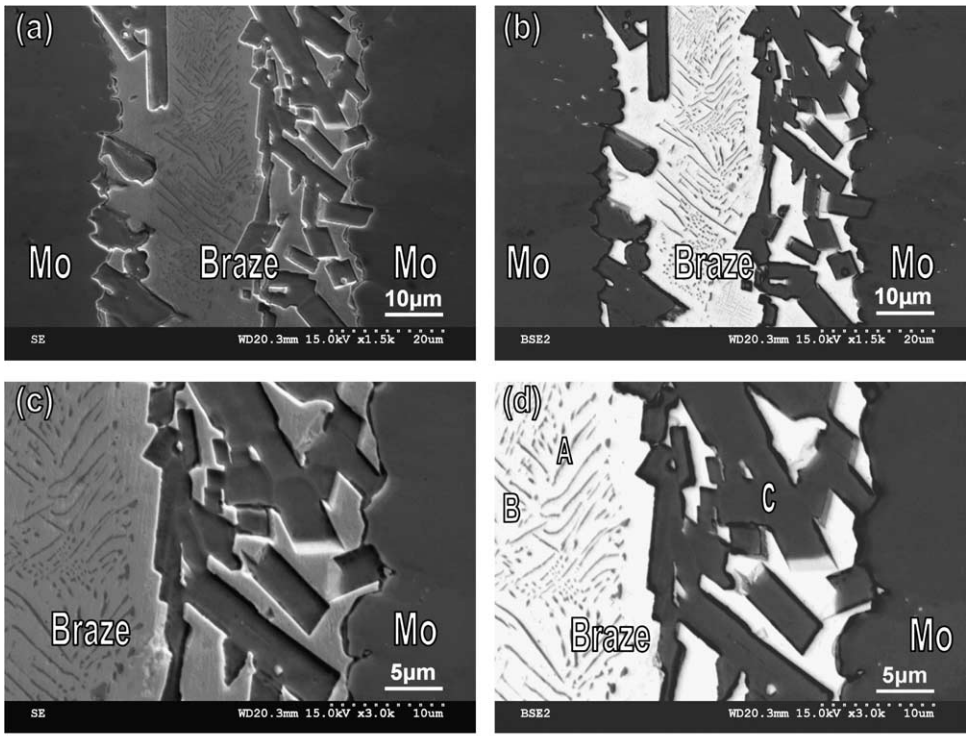

Location (phase) / at%	Au	Pd	Ni	Mo
A(Ni-rich)	12.0	6.2	79.0	2.7
B(Au-rich)	74.4	14.2	11.4	0.0
C(MoNi)	2.8	2.9	47.4	47.0

Fig. 2. The SEM: (a), (c) SEIs; (b), (d) BEIs and EDS chemical analysis results of furnace brazed joints at 1050 °C for 1200 s.

from one end of the section to the other does maintain a constant weight percentage due to different atomic numbers of Au, Ni and Pd in the ternary alloy system. For example, 10 wt% Pd can be obtained from the composition of 82.9 at% Au and 17.1 at% Pd at the left end of Fig. 4. Similarly, 10 wt% Pd can also be obtained from the composition of 94.2 at% Ni and 5.8 at% Pd at the right end of Fig. 4. In other words, a straight line in weight percent will become a curve in atomic percent for the ternary alloy phase diagram. According to the Fig. 4, the Au-rich phase can dissolve Pd and Ni, and the Ni-rich phase dissolves Pd and Au. It is expected that both Au-rich and Ni-rich phases are expected in the brazed joint. Based on Fig. 2(b) and (d), the brazed joint mainly consists of the Au-rich phase, and minor needle like Ni-rich phase separated from Au-rich matrix is also observed. It is consistent with the ternary Au–Ni–Pd phase diagram.

Based on the binary alloy phase diagram, the Au–Mo phase diagram is a simple eutectic with no intermediate phase [14]. The Au-rich matrix has the maximum solid solution of 1.25 at% Mo at the eutectic temperature of 1054 °C, and the Mo merely has the maximum solubility of 0.4 at% Au [14]. In contrast, the Ni can dissolve Mo up to 17 at% at 700 °C. Accordingly, the dissolution of Mo substrate into the Ni-rich melt is much more prominent than that of Au-rich melt. It is concluded that wetting of the Mo substrate by the molten braze is primarily attributed to the molten braze containing Ni. Additionally, the presence of interfacial angular MoNi intermetallic compound demonstrates strong metallurgical reaction between the molten braze and Mo substrate as displayed in Fig. 2. The formation of interfacial MoNi phase significantly decreases the amount of Ni content from the molten braze alloy. Although the Ni content of the braze alloy is as high as 46.5 at%, the Ni-rich phase in the brazed joint is greatly decreased after brazing.

Fig. 5 shows SEM images and EDS chemical analysis results of infrared brazed joints with various brazing conditions. The microstructure of the infrared brazed joint at 1050 °C (Fig. 5(a)–(c)) is very different from that of furnace brazed specimen (Fig. 2). The infrared brazed joint is primarily consists of the Au-rich matrix and interfacial Ni-rich as shown in Fig. 5(a)–(c). Additionally, the interfacial Ni-rich phase alloyed with Au, Pd and Mo is observed as marked by A in Fig. 5(c). It is also noted that there is no intermetallic phase found in

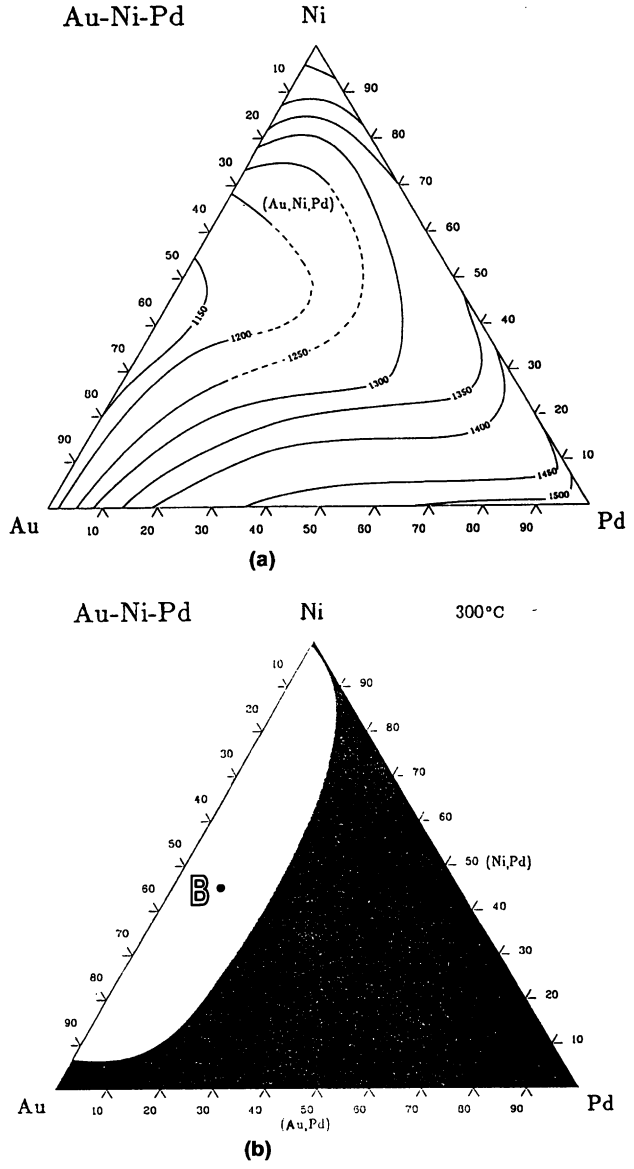

Fig. 3. Au–Ni–Pd ternary alloy phase diagrams in atomic percent: (a) liquidus projection and (b) isothermal section at 300 °C [13].

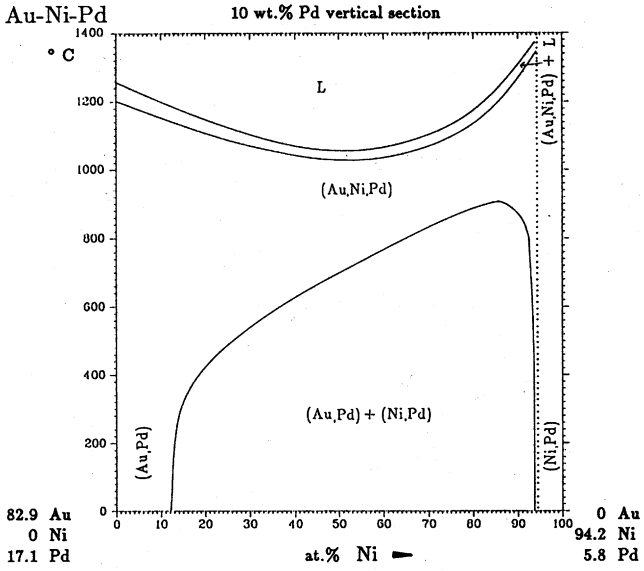

Fig. 4. 10 wt% Pd vertical section of Au–Ni–Pd pseudobinary phase diagram [13].

the figure. As described earlier, the existence of Ni-rich melt is beneficial to wettability of the molten braze on the substrate, and the Au-rich melt has little help in wetting of the Mo substrate. It is in accordance to the experimental observations.

The microstructure of the infrared brazed joint at 1100 °C for 180 s is very similar to that of infrared brazed one at 1050 °C. However, the microstructure of the infrared brazed joint at 1100 °C for 300 s is close to that of furnace brazed specimen. In addition to the Au-rich and Ni-rich phases, the interfacial MoNi intermetallic compound is extensively observed in Fig. 5(f). Strong metallurgical reactions between the braze and substrate are widely proceeded. Accordingly, its microstructure is similar to the furnace brazed specimen as compared between Fig. 5(f) and Fig. 2.

Table 2 displays shear strengths of various brazed specimens. Based on the table, all infrared brazed joints are fractured at the Mo substrate, so there is no accurate shear strength available for these infrared brazed joints. The shear strength of infrared brazed specimen shown in Table 2 reflects the shear strength of Mo substrate instead of the brazed joint. The fluctuation of experimental data for the infrared brazed specimen is probably caused by the inherent brittleness and/or defects of the Mo substrate at room temperature. In general, the shear strength of infrared brazed joint is higher than that of the furnace brazed one. Fig. 6 shows the SEM BEI cross-sectional image and SEI fractograph of the infrared brazed joint at 1050 °C for 180 s after the shear test. The braze alloy is free of crack as indicated by the arrow in Fig. 6(a). It is clear that cracks initiate and propagate along the Mo substrate, and quasi-cleavage fracture is widely observed in the fractograph as illustrated in Fig. 6(b).

Only the furnace brazed specimen is fractured along the brazed joint, and its average shear strength is 110.4 MPa. Fig. 7 shows the SEM BEI cross-sectional image and SEI fractograph of the furnace brazed joint at 1050 °C for 1200 s after shear tests. Based on Fig. 7(a), the furnace brazed joint is primarily fractured along the interfacial angular MoNi intermetallics. Cleavage dominated fracture is extensively observed in the fractured surface as illustrated in Fig. 7(b). The huge angular MoNi phase with cracks is further identified in the EDS chemical analysis as indicated by arrows in the figure. Consequently, the formation of interfacial MoNi intermetallic compound in the brazed joint is detrimen-

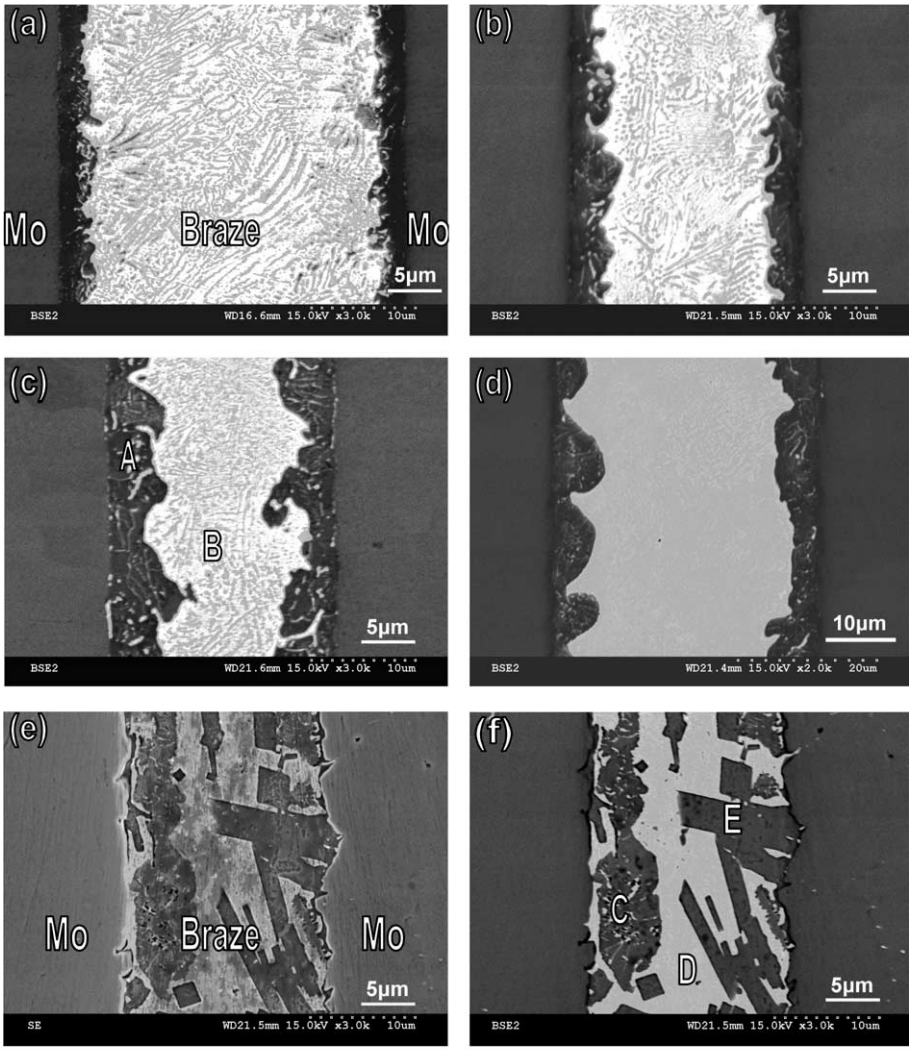

Location (phase) / at%	Au	Pd	Ni	Mo
A (Ni-rich)	7.0	5.0	82.6	5.4
B (Au-rich)	58.8	10.2	30.9	0.0
C (Ni-rich)	8.6	8.2	68.1	15.0
D (Au-rich)	66.0	11.2	22.8	0.0
E (MoNi)	3.2	3.2	47.4	46.2

Fig. 5. The SEM images and EDS chemical analysis results of infrared brazed joints: (a) BEI, 1050 for 90 s, (b) BEI, 1050 °C for 180 s; (c) BEI, 1050 °C for 300 s; (d) BEI, 1100 °C for 180 s; (e) SEI and (f) BEI, 1100 °C for 300 s.

Table 2
Shear strengths of various brazed specimens

Brazing type	Temperature (°C)	Time (s)	Shear strength (MPa)	Average Shear strength (MPa)	Standard deviation (MPa)
Furnace	1050	1200	119.2	110.4	8.9
		1200	101.5		
Infrared	1050	180	511 (fracture of the Mo substrate)		
Infrared	1050	300	303 (fracture of the Mo substrate)		
Infrared	1100	180	469 (fracture of the Mo substrate)		
Infrared	1100	300	390 (fracture of the Mo substrate)		

tal to its bonding strength. Additionally, the application of rapidly infrared brazing is a very effective way to inhibit excessive growth of the interfacial MoNi phase in the brazed joint.

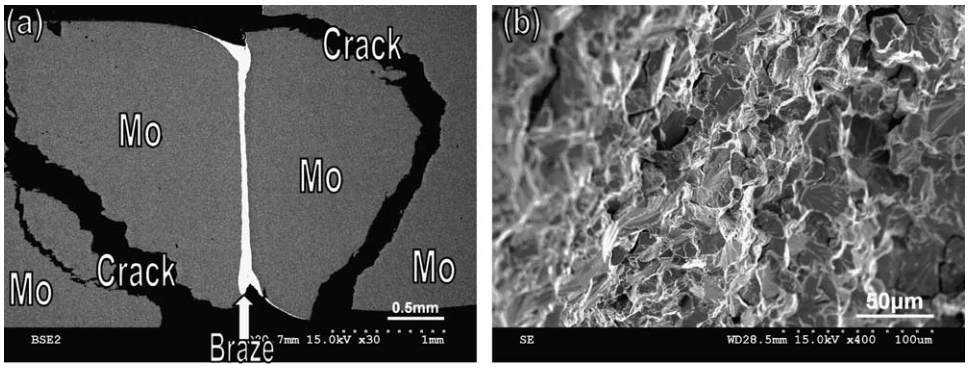

Fig. 6. The SEM: (a) BEI cross-sectional image and (b) SEI fractograph of the infrared brazed Mo/70Au–22Ni–8Pd/Mo joint at 1050 °C for 180 s after the shear test.

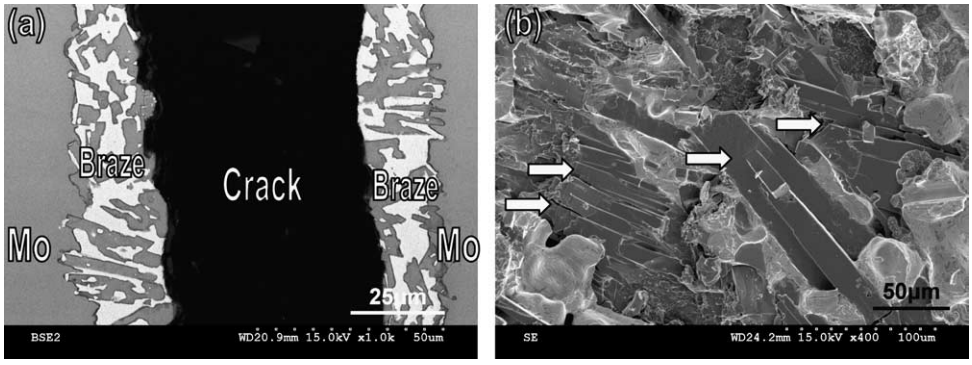

Fig. 7. The SEM: (a) BEI cross-sectional image and (b) SEI fractograph of the furnace brazed Mo/70Au–22Ni–8Pd/Mo joint at 1050 °C for 1200 s after the shear test.

4. Summary

Microstructural evolution of the brazed Mo joint using the 70Au–22Ni–8Pd braze alloy has been accessed in this study. The molten braze can effectively wet the Mo substrate above 1070 °C. Both Au-rich and Ni-rich phases are observed for the infrared brazed joint at 1050 °C. The Au-rich liquid is not reacted with the Mo substrate. In contrast, the Ni-rich liquid preferentially reacts with the Mo. With increasing the brazing temperature and/or time, the interfacial reaction between the molten braze and Mo substrate is significantly increased, and the huge angular MoNi intermetallic compound is formed in the brazed joint, especially for the furnace brazed specimen due to its slow thermal history. In general, the shear strength of infrared brazed joint is higher than that of the furnace brazed one. All infrared brazed joints are fractured at the Mo substrate, so there is no shear strength available for these infrared brazed specimens. Only the furnace brazed specimen is fractured along the brazed joint, and its average shear strength is 110.4 MPa. The formation of interfacial MoNi intermetallic compound in the brazed joint is detrimental to its bonding strength. Cleavage dominated fracture is widely observed in fractographs of the furnace brazed specimen. Additionally, the application of rapid infrared brazing is a very effective way to inhibit excessive growth of the MoNi phase in the brazed joint.

Acknowledgment

The authors gratefully acknowledge the financial support of this research by the National Science Council (NSC), Republic of China under NSC grant 93-2216-E-002-028.

References

[1] Smith WF. Structure and properties of engineering alloys. 2nd ed. New York: McGraw-Hill Inc; 1993.
[2] Davis JR. 9th ed. Metals handbook, vol. 2. Materials Park: ASM International; 1990.
[3] Schwartz M. Brazing: for the engineering technologist. Materials Park: ASM International; 1995.
[4] Chan HY, Shiue RK. The study of brazing Ti–6Al–4V and TZM alloy using pure silver. J Mater Sci Lett 2003;22:1659–63.
[5] Chan HY, Liaw DW, Shiue RK. Microstructural evolution of brazing Ti–6Al–4V and TZM using silver-based braze alloy. Mater Lett 2004;58:1141–6.

[6] Chan HY, Liaw DW, Shiue RK. The microstructural observation of brazing Ti–6Al–4V and TZM using the BAg-8 braze alloy. Int J Refract Met Hard Mater 2004;22:27–33.
[7] Hiraoka Y, Nishikawa S. Joining of single-crystalline molybdenum and carbon–ceramics by using palladium and palladium–silver alloy as brazing metal. Int J Refract Met Hard Mater 1996;14:311–7.
[8] Hiraoka Y. Brazing of single-crystalline molybdenum by using Pd–20%Ag alloy. Refract Met Hard Mater 1992;11:303–7.
[9] Hidaka Y. High-temperature annealing embrittlement of single-crystalline molybdenum joined by using Mo–40%Ru alloy. Hard Mater 1992;11:89–95.
[10] Shiue RK, Wu SK, Chen SY. Infrared brazing of TiAl intermetallic using BAg-8 braze alloy. Acta Mater 2003;51:1991–2004.
[11] Shiue RK, Wu SK, Hung CM. Infrared repair brazing of 403 stainless steel with a nickel based braze alloy. Metall Mater Trans 2002;33A:1765–73.
[12] Shiue RK, Wu SK, Chen SY. Infrared brazing of TiAl using Al-based braze alloys. Intermetallics 2003;11:661–71.
[13] Villars P, Prince A, Okamoto H. Handbook of ternary alloy phase diagrams. Materials Park: ASM International; 1995.
[14] Massalski TB. Binary alloy phase diagrams. Materials Park: ASM International; 1990.